EDDY SIMULATION OF COMPOUND CHANNEL, WITH ONE FLOODPLAIN

Rawya Monir Kansoh
Hydraulics and Irrigation Engineering Department Faculty of Engineering,
Alexandria University, Alexandria, Egypt.

ABSTRACT

Eddy simulation of flow in a compound open channel with one floodplain has been analyzed. The results are in good agreement with the experimental measurements and previous numeric results. The secondary circulation field, bed stress distribution and lateral stress distribution are being presented.

Keywords: Boundary shear, hydraulics of channels with floodplains, secondary currents, turbulence modelling, circulation of compound open channels.

1. INTRODUCTION

The hydraulic characteristics of open channels with floodplains have important applications in river management, flood control, and irrigation, yet are difficult to model because the interaction between the main channel and the floodplain is relatively complex.

A number of experimental measurements of the mean velocity and boundary shear stress has been made using Pilot static and Preston tube probes, see for example Myers & Elsawy [1], Rajaratnam & Ahmadi [2], Knight & Demetriou [3], Knight & Hamed [4], and Nalluri & Judy [5]. More detailed experimental measurements including turbulence quantities and secondary currents have been made by Tominaga & Ezaki [6], Tominaga et al. (7) using hot-film probes, and by Arnold et al. [8], Tominaga et al [9], Shiono & Knight [10], and Tominaga & Nezu [11] using laser doppler anemometers. Recent numerical calculations using an algebraic stress model and k - ϵ transport equations have been performed by Krishnappen & Lau [12], Naot, Nezu & Nakagawa [13], and Naot, Nezu & Nakagawa [14].

The present paper describes a new numerical calculation of turbulent flow in a compound open channel using the Large Eddy Simulation (LES) technique. The method is closely related to Direct Numerical Simulation (DNS) but differs in that only the large eddies or grid-scales are explicitly retained with the sub-grid scales being represented by a subgrid model (SGM), thus the computer resources needed are much lower. Although the method is dependent on a model, experience shows that the computed results are relatively insensitive to the model details.

2. MATHEMATICAL FORMULATION

Consider turbulent incompressible flow maintained by gravity g in the compound channel shown. The main section is of width b and depth H with a floodplain section on one side raised a height h above the main bed and extending the total width to B. The floodplain geometry is characterised by the depth ratio $D_r = (1 - h/H) = 0.5$, the width ratio $B/h = 3$ and the overall aspect ratio $B/H = 5$. The average flow is assumed uniform in the streamwise direction so that the bed slope S_o and energy slope I_e are the same, hence the average value of the kinematic wall shear stress τ_w acting on the channel sides and bottom is given by

$$\tau_w \equiv u_T^2 = gRS_o = gRI_e \qquad (1)$$

where u_T denotes the average friction velocity and

R denotes the hydraulic radius R = 15H/28. The overall Reynolds number R_e is given by

$$R_4 \equiv \frac{4U_b R}{\nu} = \frac{1.5U_b}{\tau u_r}\frac{Hu_r}{\nu} \qquad (2)$$

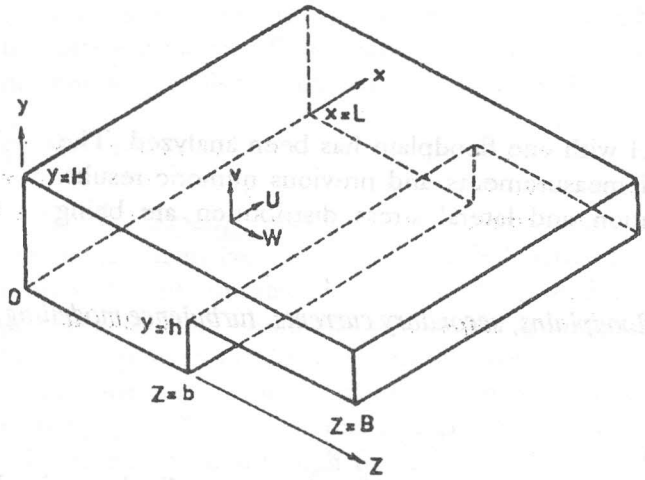

Figure 1. Channel geometry and coordinate system.

where ν denotes the kinematic viscosity. The bulk velocity U_b is determined from the simulation and the quantity $H^+ = Hu_\tau/\nu$ is a characteristic determinant of the flow and reflects the ratio of length scales between the large scale turbulent structure and the small scale wall length ν/u_2. It is convenient to non-dimensionalies certain quantities using a wall length scale which will be indicated by a super-script (+). In the present simulation we have set $H^+ = 1000$ and determine that $R_e \sim 42000$. The channel is assumed to be hydraulically smooth. The Kolmogarow length scale $\eta = (\nu/\epsilon)^{1/4}$ can be estimated if we approximate the dissipation rate $\epsilon \sim u_\tau U_b/H$ and suppose that $U_b/m_\tau \sim 20$ hence $\eta_2(H^+/20)^{1/4}$ or about 2.6 wall units. A direct simulation of this channel would therefore require about 380 cells vertically, 1900 laterally and (say) 2000 streamwise; while this is not impossible it is reasonable to make a first exploration with a large eddy simulation at a much lower resolution. The characteristic time scale of the large eddies in the main channel is H/u_1, the floodplain has a time scale of half this and so develops more quickly, but the overall time scale is determined by the lateral development which is about B/H times H/u_1. The magnitude of the secondary current velocity is about 0.5 u_1, so the time required to convect across the floodplain is about B/u_1 as before. The channel length required can be estimated in an experiment for the flow to reach full lateral development by considering the mean distance the fluid travels in one characteristic time H/u_1, this equals 186 hydraulic radii.

2.1 Numerical methods

The velocity field $u_i = (u, v, w)$ satisfies a discrete form of the Navier-Stokes Equations obtained by a second order finite difference method applied to a staggered grid. The arrangement is similar to that used by Schumann [15] and conserves momentum and kinetic energy but is extended to allow non-uniform grid spacing in the channel cross-section. The time advancement is by second order. Adams-Bashforth method. Let us define the quantity

$$H_i^n = \left[-\frac{\delta n_i u_j}{\delta x_j} + \frac{\delta \tau_{ij}}{\delta xj} + g_i\right]^n \qquad (3)$$

where n denotes the discrete time level, δ the finite difference operator, τ_{ij}, the combined viscous and subgrid stress. The solution is advanced over a time step using the equations

$$\frac{\hat{u}_i - u_i^n}{\Delta t} = \frac{3}{2}H_i^n - \frac{1}{2}H_i^{n-1} + \frac{1}{2}\frac{\delta P^{n-1}}{\delta z_i} \qquad (4)$$

$$\frac{u_i^{n+1} - \hat{u}_i}{\Delta f} = -\frac{3}{2}\frac{\delta p^n}{\delta z_i} \qquad (5)$$

$$D^2 p^n = \frac{2}{3\Delta t}\frac{\delta \hat{u}_j}{\delta x_j} \qquad (6)$$

where p denotes the pressure, $\hat{u}_i$, an intermediate variable, Δt the time step, and D^2 the discrete Laplace operator. Equation (6) is equivalent to the continuity equation $\delta u_j/\delta x_j = 0$. First $\hat{u}_i$, is computed using (4), then continuity at time level n + 1 is enforced by solving the Poisson equation (6) for the pressure using the cyclic reduction algorithm of

Swartztrauber [16]. The u_j^{n+1} velocity is completed using equation (5).

We avoid having to specify inflow and outflow conditions by assuming that the flow field is periodic in the streamwise direction with a repeat length L; this is consistent with fully developed channel flow provided that the flow is spatially uncorrelated over distances of L/2. The two dominant mechanisms, whereby extended spatial correlations, are maintained: large scale eddy structure which is known to extend for few times the depth, and slow speed streaks near to the walls which extend for about a thousand wall units. In both cases it is sufficient to take L = 6H although at lower Reynolds numbers the streak length will demand a relatively longer box. The final simulation was run with 32 cells vertically, 127 cells laterally (64 in the main channel and 63 in the floodplain), and 127 cells along the channel. The lateral resolution is restricted to the form 2^m -1, where m is an integer, by the cyclic reduction algorithm, but the mesh was stretched slightly to force square cells in the channel corners. The mesh intervals are $\Delta x^+ = 47$, $\Delta y^+ \simeq 31$, $\Delta z \cong 39$; thus the resolution extends down to about 13 Kolmogarow lengths. It follows that the nearest point to the wall are about 16 wall units away and outside the laminar sublayer but not within the logarithmic region. The wall treatment is given in some detail in § 2.4.

At the free surface, a rigid stress free lid is being imposed and thus ignore the presence of surface waves or free surface deformations. The simulation is therefore independent of the Froude Number but the results will be applicable only to physical systems where $F_r = U_b/\sqrt{gH}$ is small or wave effects are relatively weak.

The simulation was started in a half resolution box (63 x 16 x 63) from an initial constant profile with an artificial turbulence field composed of random numbers. It was integrated over time for about $80H/u_t$, transferred to the final (127 x 63 x 127) box, and integrated for a further $80H/u_T$ keeping the convection Courant number $u\Delta t/\Delta x \sim 0.1$. The flow was considered fully developed when successive plots of the bed shear stress had converged. The simulation was then run for another 30 H/u_t to gather turbulence statistics.

2.2 *Internal Surface Implementation*

The compound geometry of the main channel and floodplain present some difficulty for the efficient numerical solution of the Poisson equation (4) turbulence simulations require fast numerical algorithms with operation counts approaching O(m log m), where m denotes the number of unknowns, and these are available only for simple geometric configurations. To circumvent this problem while still maintaining the O (m log m) operation count we use an approximate method based on the observation that the change in pressure gradient at any point from one time step to the next is relatively small compared with a typical value. Although this appears very crude the method when combined with a small number of iterations appears to work well. Specifically, we use an extended computation box and define the channel walls by imposing an impermeable surface along a fixed path within the box. On this surface we apply the usual shear stress boundary conditions but also enforce an approximate no-flux boundary condition. First, we save a copy of the normal pressure gradient $\delta p/\delta I_w$, at all points on the internal surface, and use this value to offset the u computed in equation (2), then we solve equation (4) using a fast solver and compute u_i^{n+1} using (3). If the offset was correct we would have a zero normal velocity at time n + 1 on the internal surface but in practice we find that a small number of interations are necessary.

2.3 *Subgrid Parameterisation*

The contribution of the unresolved subgrid motions to the stress is modelled by the standard Smagorinsky [17] method.

$$T_{ij} = 2(\nu + \nu_3)\, S_{ij} \tag{7}$$

$$S_{ij} = \frac{1}{2}\left(\frac{\delta u_i}{\delta x_j} + \frac{\delta u_j}{\delta x_i}\right) \tag{8}$$

$$\nu_3 = l_3^2\, (2S_{ij}\, S_{ij})^{1/2} \tag{9}$$

where the subgrid eddy viscosity ν_3 is related to the rate of deformation S_{ij} using a simple mixing length model. The subgrid length scale I_s depends on the

finite difference grid spacing, and for a non-cubic mesh is given by the expression due to Deardorff [18].

$$l_s = C_o (\Delta x\, \Delta y\, \Delta z)^{1/3} \quad (10)$$

in which C_o is the Smagorinsky constant. The Smagorinsky constant C_o is the only adjustable parameter in the subgrid model and lies in the approximate range 0.094 to 0.2 although the simulation results are relatively insensitive to its value. Lilly (1966) determined on theoretical grounds that for homogenous turbulence $C_o = 0.17$, however in the presence of a mean shear rate Deardorff [18] found that this value resulted in excessive damping of large scale motions and used $C_o = 0.094$. Piomelli, Moin & Ferziger [19], and later researchers have found that the optimum value is approximately 0.1, and the present simulation is performed using $C_o = 0.095$. Near to a solid boundary the length scale is reduced and ultimately must scale on the usual mixing length Kl_w, where K denotes von Karman's constant and l_m denotes the distance to the wall, and be independent of the finite difference grid spacing. We have used the simple matching rule that l_o is taken as the smaller of the two values, ie. that

$$l_3 = \min (C_o(\Delta x \Delta y \Delta z)^{1/3}, Kl_w \Gamma(l_w^+)) \quad (11)$$

$$\Gamma(l_w^+) = 1 - \exp (- l_w^+/A^+) \quad (12)$$

where Γ is the standard Van Direst [20] damping factor.

2.4 Bed and Sidewall Boundary Conditions

The stress boundary condition applied on the walls of the channel is similar to that used by Schumann [15] in which the instantaneous stress τ is assumed to vary in phase with the instantaneous velocity u, but modified in a manner analogous to Grotzbach [21] to allow the ratio to vary over the cross-section. i.e.

$$\frac{\tau}{\tau_a} = \frac{u}{u_a} \quad (13)$$

where τ_a and u_a represent averages taken over a streamwise strip at a point on the channel perimeter and over time as defined below. These are not independent but are related by the usual turbulent velocity profile f which is known with increasing accuracy as the wall is approached, ie.

$$u_a = (\tau_a) 1/2 f(l_w^+) \quad (14)$$

$$l_w^+ = (\tau_a) 1/2 l_w^+/\nu \quad (15)$$

where l_w is the distance of the nearest velocity point from the wall. The function $f(l_w^+)$ is defined by a logarithmic curve fit to the universally accepted velocity profile, see for example Goldstein [22]. The scheme reduces to the usual laminar no-slip boundary condition when $l_w^+ < 5$. We compute u_a from the history of the local flow field using

$$T\frac{d}{dt}u_a + u_a = \frac{1}{L}\int_a^L u\,dx \quad (16)$$

where T denotes the characteristic time of the averaging process and initially $u_a = u(0)$. Typically T is or order H/u_2; it must be large compared with typical turbulent fluctuations but small enough to allow convergence of the bed stress in a reasonable time. Experience shows that it has little effect on the simulation. Given u_a, we solve equations (14) and (15) for l_w^+ using an efficient bisection scheme and thus determine τ_a. This scheme enables the first mesh point to be placed outside the laminar sublayer and allows the bed stress to vary in an arbitrary way across the channel while still being determined from the simulation rather than set a priorities.

2.5 Mean Velocity and Secondary Circulation

Tominaga & Nezu [11] have carried out an experimental study of an identical compound channel at a Reynolds number Re = 54500, and hence $H^+ = 1195$, which is close the that of the simulation. They used a fiber-optic laser doppler anemometer to measure three components of turbulent velocity in a test section 174 hydraulic radii downstream of the inlet plain and 116 hydraulic

radii upstream of the outlet device. Although this inlet length appears insufficient to allow for proper lateral development the results are useful for comparison.

The mean streamwise velocity normalized by u_T is shown in Figure (2). The maximum velocity U_m of 24.5 u, occurs near the centre line of the main channel at about 2/3 of the depth. The bulk velocity U_b equals 19.4 u_τ which implies a simulation Renolds number of R_e = 41571. The experimentally measured values of maximum velocity and U_b are 23.7 u_T, and 21.3 u_T, respectively, these are in good agreement with the simulation and the higher experimental value of U_b is consistent with an underdeveloped velocity profile.

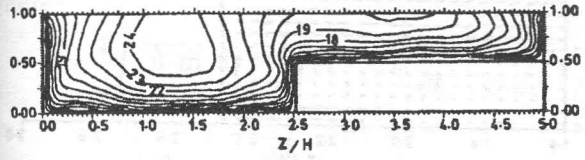

Figure 2. Mean velocity distribution $\bar{u}/u^*$.

1. Mean velocity distribution

Figure (3) shows the computed mean velocity profile non-dimensionalised by the local u^* at the centreline of the main channel plotted against the local value of $y^+ = yu^+/\nu$. The computed profile shows a logarithmic region up to about $y^+ \simeq 600$ with a peak at $y^+ \simeq 750$ corresponding to y/H $\simeq$ 0.67. The experimentally measured (Nezu & Rodi, [24]) profile for a wide open channel at a Reynolds number of R_e = 55000 is shown for comparison. Also included are the measurements of Tominaga & Nezu [11]. Both experimental profiles are close to the logarithmic profile

$$\frac{u}{u^*} = \frac{1}{\kappa} \ln y^+ + 5.29 \qquad (17)$$

appropriate for a wide open channel but differ in the wake region. The Tominaga & Nezu [11] measurements are constrained to this profile because their data reduction technique determines the bed stress, and hence the local u^*, by fitting equation (17) using a least squares method rather than making an independent measurement. This technique has been shown by Nezu & Rodi [24] to be satisfactory for wide channels but its usefulness for narrow channels is not yet established. It has been suggested, (see Gavrilakis [23]), that the logarithmic profile (based on local shear velocity) found for turbulent flow in a square duct exhibits a logarithmic region similar to equation (17) but with different constants (also shown in figure (4)). We would expect that the profile for the present channel should be intermediate between the square duct and the wide channel.

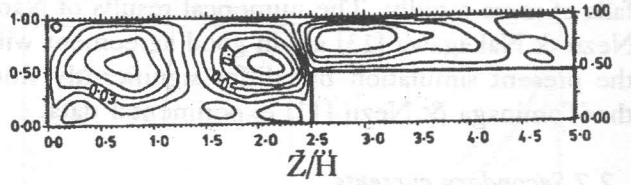

Figure 3. Mean velocity $\bar{u}/u^*$ profile at centre of main channel made non-dimensional using local u^* value.

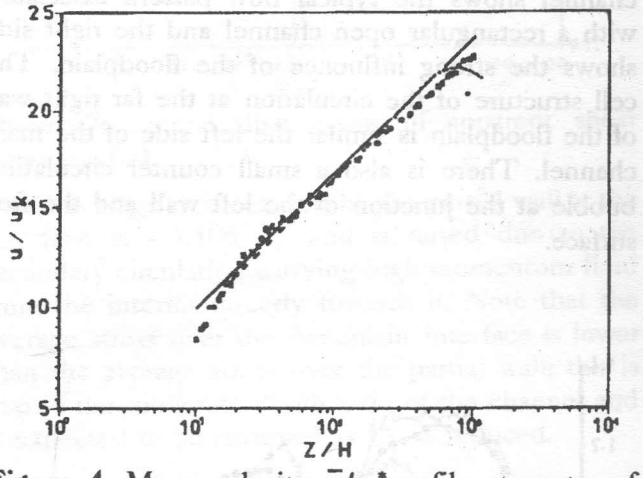

Figure 4. Mean velocity $\bar{u}/u^*$ profile at centre of main channel made non-dimensional using local u^* value.

2.6 Bed Shear stress distribution

The distribution of bed shear stress made non-dimensional using u_T^2 across the main channel and floodplain is shown in Figure (4). The main channel profile has a maximum of 1.28 u_T in the centre and a local peak at z/H $\simeq$ 0.15 associated with the lower secondary flow cell at the corner. There is another

local peak at the opposite corner but this is less well defined. The bed stress values determined by Tominaga & Nezu [11] are lower and do not extend as far into the corners. The simulated results however are in good agreement with the numerical calculation of Naot, Nezu & Nakagawa [13] for the same channel performed using a k - ϵ model. The bed stress distribution on the floodplain has a maximum value of 1.13 u_T, at the channel junction and with distance across the floodplain. The Tominaga & Nezu [11] values attain a higher peak of $1.2u_T$, slightly away from the junction and then falls of more rapidly. The numerical results of Naot, Nezu & Nakagawa [13] are in good agreement with the present simulation but differ significantly from the Tominaga & Nezu [11] experimental data.

2.7 Secondary currents

The distribution of mean velocity within the cross-section reflects the influence of the secondary circulation shown in Figure (5). The left side of the channel shows the typical flow pattern associated with a rectangular open channel and the right side shows the strong influence of the floodplain. The cell structure of the circulation at the far right wall of the floodplain is similar the left side of the main channel. There is also a small counter circulation bubble at the junction of the left wall and the free surface.

Figure 5.. Distribution of bed stress τ_b/w^2 across the main channel and floodplain.

Figure (6) shows the secondary velocity vectors in the interface region. The dominant feature is the strong up flow inclined at an angle of 20 degrees from the vertical and originating from the junction corner; it separates the circulation systems of the main channel and the floodplain and contains the maximum velocity of 0.9 u_T (3.7 % of U_m).

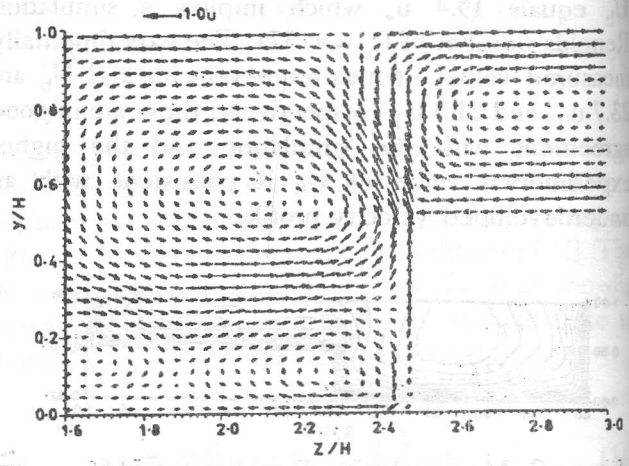

Figure 6. Vector plot of secondary circulation in the interface region.

The combined mass flux is approximately 57 % due the main channel and 43 % due to the floodplain. The surface separation point is located approximately 0.14 H away from the interface towards the main channel; the typical secondary velocity at the surface at some distance from the separation point is about 0.5 u_t in the main channel and 0.78 u_t in the floodplain. The mid channel surface stagnation point dividing the left and right side circulations of the main channel is located at z = 1.4 H. In the main channel there is a strong lateral flow towards the interface wall originating from the high velocity interior and ending in a stagnation point at about y = 0.25 H. This lateral flow is responsible for increasing the wall stress on the interface wall. The floodplain circulation has developed into a relatively wide cell and is responsible for the transport of streamwise momentum well into the floodplain. The secondary circulation is in good agreement with the measurements of Tominaga & Nezu (1991) but the lateral extent of the floodplain circulation cell is greater in the simulation.

3. DISTRIBUTION OF LATERAL MOMENTUM TRANSFER

In an open channel the local bed shear stress τ_b is modified from its wide channel value gdS_o where d denotes the local depth, by the lateral gradients in apparent shear stress T_a acting on vertical planes aligned with flow direction and averaged over depth. It is convenient to split r_a into two components T and J representing the turbulent diffusive transport and secondary current transport, respectively. The depth averaged equation for streamwise momentum is given by

$$gdS_o - \tau_b + \frac{\partial}{\partial z}(Td + Jd) = 0 , \qquad (18)$$

where

$$T = \frac{1}{d}\int -\overline{\tilde{u}\,\tilde{m}}\, dy + \frac{1}{d}\int (\nu + \nu_t)\left(\frac{\delta \bar{u}}{\partial z} + \frac{\partial \bar{w}}{\partial x}\right) dy \qquad (19)$$

$$J = \frac{1}{d}\int -\bar{u}\bar{w}\, dy \qquad (20)$$

and the viscous and subgrid terms have been summed up with the T component. The wide channel values are $gHS_o = 1.866u_t^2$ and $g(H - h)\, S_o = 0.933u_T^2$ for the main channel and floodplain respectively and the τ_b profile is shown in Figure (4). The lateral distribution of τ_a, T, and J are plotted in Figure (7), the T profile is plotted twice, once with and once without the subgrid terms which are significant only at the sidewalls. In the main channel, τ_o has developed a monotonic profile with nearly constant slope in the centre region and sign change at z/H = 1.15 and the expected asymmetry due to the floodplain is relatively weak, the left sidewall value is $0.9334u_t^2$ and the average value over the interface partial right wall is - $0.907\ u_t^2$. The asymmetry is much stronger in the separate component T and J, partially because J is not forced to zero at the sidewall boundary. The apparent stress in the main channel is carried mostly by the Reynolds stress. In the flood plain the apparent stress is always of the same sign (-ve) with a local extremum at z/H = 4.3, where the bed stress τ_b equals the wide channel value and a right sidewall value of - $0.561u_\tau^2$. Over most of the floodplain the apparent stress is carried mostly by the secondary current component J except near to the right sidewall and very close to the interface where the Reynolds stress component T dominates. Very close to the interface on the main channel side a curve drawn between the junction corner and the surface stagnation point marks the separation line between the circulation systems of the main channel and floodplain; the momentum transport across this must be wholly due to the Reynolds stress and hence the ratio of T to J must vary rapidly in the floodplain as the interface is approached. It also follows that on the main channel side J is forced to small non-zero extremum close to the interface.

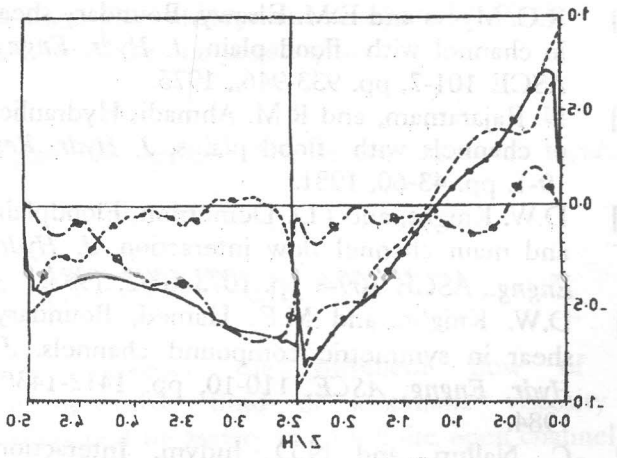

Figure 7. Lateral distribution of apparent shear stress τ_a=T+J.

The average stress carried by the partial wall at the interface is - $1.106\ u_\tau^2$ and is raised due to the secondary circulation carrying high momentum fluid from the interior directly towards it. Note that the average stress over the floodplain interface is lower than the average stress over the partial wall; this is due to the moderate depth ratio of the channel and is expected to be reversed as D_t, is reduced.

4. CONCLUSIONS

A successful simulation has been carried out of a rectangular channel with a flood-plain. This simulation has reproduced the complex flow patterns associated with this geometry. Of particular interest is the secondary flow at the internal corner and the increase in the bed stress on the floodplain. The latter phenomenon results from the lateral transfer of momentum from the main channel by the extended secondary circulation existing on the floodplain. Overall, good agreement has been obtained with the

experimental data, but more detailed comparisons have not proved worthwhile.

Small differences between the simulation and experimental results may be attributed to (i) the experimental bed stress, and also overall energy slope I_e, which is used to drive the simulation , was not measured directly but deduced from an assumed velocity profile, and (ii) possibly insufficient inlet length for the full development of the secondary circulation pattern (particularly over the floodplain).

REFERENCES

[1] R.C. Myers and E.M. Elsawy, Boundary shear in channel with flood plain, *J. Hydr. Engng*, ASCE 101-7, pp. 933-946., 1975.

[2] N. Rajaratnam, and R.M. Ahmadi, Hydraulics of channels with flood plains. *J. Hydr. Res.* 19-1, pp. 43-60, 1981.

[3] D.W. Knight, and J.D. Demetrion, Floodplain and main channel flow interaction, *J. Hydr. Engng.*, ASCE 109-8 pp. 1073-1092, 1983.

[4] D.W. Knight, and M.E. Hamed, Boundary shear in symmetric compound channels. *J. Hydr. Engng, ASCE*, 110-10, pp. 1412-1430, 1984.

[5] C. Nalluri, and N.D. Judym, Interaction between main channel and flood plain flow. Proc. 21st Congg. LAHR Melbourne, Australia, pp. 378-382, 1985.

[6] A. Tominags, and K.K. Ezaki, Hydraulic characteristics of compound channel flow. *Proc. 6th Cong. of Amin and Pacific Din., IAHR*, Kyoto, Japan, pp. 465-472, 1988.

[7] A. Tominaga, I. Nezu, K. Ezaki and H. Nakagawa, Three-dimensional turbulent structure in straight open channel flows. *J. Hydr., Res.* 27.1 pp. 149-173, 1989.

[8] U. Arnold, J. Stein and G. Rouve, Sophisticated measurement techniques for experimental investigation of compound open channel flow. Computational Modeling and *Experimental Methods in Hydraulics. Elsevier, Dubrovnik, Yugoslavia*, pp. 11-21. 1989.

[9] A. Tominaga, I. Nezu, and K. Ezaki, Experimental study on secondary currents in compound open channels. *Proc. 23rd Cong. LHR Ottawa, Canada*, pp. A15-A22, 1989.

[10] K. Shinono and D.W. Knight, Transverse and vertical Reynolds stress measurements in a shear layer region of a compound channel. *Proc. 7th Symp. Turb. Shear Flows Stanford, Calif*, pp. 28.1.1 - 28.1.6, 1989.

[11] A. Tominaga, and I. Nezu, Turbulent structure in compound open channel flows. *J. Hydr, Engng., ASCE* P.117-1 21-40, 1991.

[12] B.C. Krishnappan and Y.L. Lau, Turbulence modelling of floodplain flows. *J. Hydr. Engng., ASCE*, pp. 112-4 251-267, 1986.

[13] D. Naot, I,m Nezu and H. Nakagawa Hydrodynamic behaviour of compound rectangular open channels. *J. Hydr. Engng., ASCE*, 119-3 pp. 390-408, 1993.

[14] D. Naot, I. Nezu, and H. Nakagawa, Calculation of compound open channel flow. *J. Hydr, Engngm ASCE*, 119-12, pp. 1418-1426, 1993.

[15] U. Schumann, Subgrid-scale model for finite difference simulations of turbulent flows in plane channels and annuli. *J. Comp. Phys.* 18-pp. 376-404, 1975.

[16] P.N. Swarztrauber, A direct method for the discrete solution of separable eliptic equations. SIAM, *J. Numer. Anal.* 11, pp. 1136-1150, 1974.

[17] J. Smagorinsky, General circulation experiments with the primitive equations, I. *The basic experiment. Mon. Weather Rev*, 91 1963, pp. 99-164, 1963.

[18] J.W. Deardorff, A numerical study of three-dimensional turbulent channel flow at large Reynolds numbers. *J. Fluid Mech.* 41, pp 453-480, 1970.

[19] U. Piomelli, P. Moin and J.H. Ferziger, Model consistency, in large eddy simulation of turbulent flows. *Phys. Fluids 31* pp. 1884-1891, 1988.

[20] E.R. Van Driest, On turbulent flow near a wall. *J. Aero, Sci.* 23, pp. 1007-1-11, 1956.

[21] G. Grotzbach. in *Encyclopedia of Fluid Mechanics*, 6, *ed. Cheremisinoff, N.P., Gulf, West Orange, Nj*, 1987.

[22] S. Goldstein, *Modern developments in fluid dynamics, Dover, NY*, 1965.

[23] S. Gavrilakis, Numerical simulation of low Reynolds number turbulent flow through a straight square duct. *J. Fluid Mech.* 244 pp. 101-129, 1992.

[24] I. Nezu, W. Rodi, Open channel flow measurements with a laser-doppler anemometer. *J. Hyd. Engng. ASCE*, 112-5 pp. 335-354, 1986.